Revisiting spin cycloids in multiferroic BiFeO_{3}

Bin Xu, Bertrand Dupé, Changsong Xu, Hongjun Xiang, and L. Bellaiche

Phys. Rev. B **98**, 184420 — Published 19 November 2018

DOI: 10.1103/PhysRevB.98.184420

Revisiting spin cycloids in multiferroic $BiFeO_3$

Bin Xu,[1,2,*] Bertrand Dupé,[3] Changsong Xu,[2] Hongjun Xiang,[4,5] and L. Bellaiche[2,†]

[1] *School of Physical Science and Technology, Soochow University, Suzhou, Jiangsu 215006, China*
[2] *Physics Department and Institute for Nanoscience and Engineering, University of Arkansas, Fayetteville, Arkansas 72701, USA*
[3] *Institute of Physics, INSPIRE Group, Johannes Gutenberg-University Mainz, 55128 Mainz, Germany*
[4] *Key Laboratory of Computational Physical Sciences (Ministry of Education), State Key Laboratory of Surface Physics, and Department of Physics, Fudan University, Shanghai, 200433, China*
[5] *Collaborative Innovation Center of Advanced Microstructures, Nanjing 210093, P. R. China*

(Dated: October 16, 2018)

We revisit the inverse spin current model that has been previously used to explain the existence of magnetic cycloids in bulk multiferroic $BiFeO_3$. Using a first-principles-based effective Hamiltonian method, and in combination with Monte Carlo simulations, we predict a magnetic phase diagram as function of first- and second-nearest-neighbor interaction strength in the spin current model, and show that, in contrast with previous understanding, both first and second nearest neighbors have to be taken into account to be in accordance with experimental findings, including the existence of type-1 and type-2 cycloids with, respectively, $[1\bar{1}0]$ and $[11\bar{2}]$ propagation directions, and the cycloid-to-antiferromagnetic transition under magnetic field. Other previously unknown magnetic arrangements are found in this phase diagram. The microscopic origins of all its magnetic phases are further explained in terms of coexistence of single solutions of the spin current model having different weights (in magnitude and even sign).

PACS numbers: 75.25.-j, 75.40.Mg, 77.80.-e

I. INTRODUCTION

Magnetic structure is a very intriguing property of a material, which is of interest for both fundamental understanding and technological applications. Various types of interactions can play roles to affect the magnetic configuration, and they can be further manipulated by external stimuli, such as temperature, pressure, fields, strain, etc. Usually, exchange interactions are dominant to determine whether the couplings between magnetic atoms are ferromagnetic (FM) or antiferromagnetic (AFM), while Dzyaloshinskii-Moriya (DM) interaction can cause spin canting or other non-collinear orderings[1,2], which is a recognized source of exotic magnetic structures in multiferroics, i.e., a system processing both electric and magnetic orderings.

One of the systems that has been under scrutiny is $BiFeO_3$ (BFO), which is likely the most studied room-temperature multiferroic. The structural ground state of bulk BFO is the $R3c$ phase, which has a large polarization in the [111] direction, together with oxygen octahedral tilting in an $a^-a^-a^-$ pattern (in Glazer's notation[3]) about the same direction. Below the Néel temperature of 640 K, it is approximately G-type AFM (G-AFM), while modulated with a complex spin cycloid propagating in one of the $< 1\bar{1}0 >$ directions (type-1 cycloid), with a period of 62 nm[4]. The formation of the cycloidal structure can be explained by a DM-type interaction, i.e., the so-called inverse spin current model[5–7], with which polarization affects the magnetic structure. The coupling energy in this model is given by $-C(\mathbf{P}\times\hat{\mathbf{e}}_{ij})\cdot(\mathbf{m}_i\times\mathbf{m}_j)$, where $\mathbf{P}$ is the polarization, $\hat{\mathbf{e}}_{ij}$ is the unit vector in the direction from site i to j, $\mathbf{m}_i$ and $\mathbf{m}_j$ are the magnetic moments at these two sites, and C is the interaction strength.

This cycloid phase appears to be energetically competing with the G-AFM state, as evidenced by a transition from type-1 cycloid to G-AFM under small compressive strain[8], magnetic field[9–12], electric field[13,14], doping[15], and hydrostatic pressure[16], strongly suggesting that these two phases are close in energy. Recently, a different (type-2) cycloid has been found in slightly tensile-strained (001) film[8] and (110) film on $SrTiO_3$ substrate[17,18], which was proposed to propagate in the $[11\bar{2}]$ direction. Type-2 cycloid is therefore also expected to be energetically close to the other two aforementioned magnetic arrangements.

A theoretical description to understand these experimental results is desired. Based on the spin current model and incorporating other magnetic interactions, previous calculations showed that type-1 cycloid can be reproduced as the ground state for bulk BFO[7,19,20], and the transition from type-1 cycloid to the G-AFM state under magnetic field can also be explained[21]. However, these studies consider either only the first nearest neighbors (NN)[20] or only the second NN in the spin current model[7,19,21]. To the best of our knowledge, this apparent discrepancy has not been addressed. Furthermore, a theoretical explanation for the existence of this type-2 cycloid is currently lacking. Given the importance of the magnetic structures of BFO, it is of great interest to answer the following questions: (i) is it necessary to take into account both 1st and 2nd NN terms in the spin current model to reproduce experimental data? (ii) what are the magnetic structures for various contributions from these two sets of neighbors? In particular, are there other complex magnetic arrangements awaiting to

be discovered? and (iii) how to understand, at a microscopic level, the existence of type-2 cycloid (and other hypothetical magnetic configurations, if any)?

This manuscript is organized as follows. Details of the computational method is provided in Section II. In Section III we present the predicted magnetic phase diagram, and how individual solutions (different first and second nearest neighbors) of the inverse DM interactions work together to produce a variety of cycloids. Finally, the study is summarized in Section IV.

II. METHODS

In this Letter, we address the aforementioned questions by using a recently developed effective Hamiltonian scheme for BFO[7]. The total energy can be expressed as a sum of two main contributions: $E_{\text{FE-AFD}}(\{\mathbf{u}_i\},\{\eta_H\},\{\eta_i\},\{\boldsymbol{\omega}_i\})$ and $E_{\text{Mag}}(\{\mathbf{m}_i\},\{\mathbf{u}_i\},\{\eta_i\},\{\boldsymbol{\omega}_i\})$, where $E_{\text{FE-AFD}}$ contains energy terms arising from non-magnetic variables, including the local mode ($\mathbf{u}_i$) being proportional to the electric dipole[22,23], the homogeneous (η_H) and inhomogeneous strain (η_i)[23], and the antiferrodistortive (AFD) mode ($\boldsymbol{\omega}_i$)[24]. The second term E_{Mag} is related to magnetism. It includes the mutual interaction between magnetic moments of Fe ions ($\mathbf{m}_i$) with a fixed magnitude of $4\,\mu_{\text{B}}$ (as consistent with first-principles calculations and measurements[25,26]) as well as couplings between magnetic moments and other degrees of freedom. Technically, the analytical form of E_{Mag} can be expressed as[7]:

$$
\begin{aligned}
E_{\text{Mag}}(\{\mathbf{m}_i\},\{\mathbf{u}_i\},\{\eta_i\},\{\boldsymbol{\omega}_i\}) = & \sum_{ij\alpha\gamma} Q_{ij\alpha\gamma} m_{i\alpha} m_{j\gamma} + \\
& \sum_{ij\alpha\gamma} D_{ij\alpha\gamma} m_{i\alpha} m_{j\gamma} + \sum_{ij\alpha\gamma} E_{ij\alpha\gamma\nu\delta} m_{i\alpha} m_{j\gamma} u_{i\nu} u_{i\delta} + \\
& \sum_{ij\alpha\gamma} F_{ij\alpha\gamma\nu\delta} m_{i\alpha} m_{j\gamma} \omega_{i\nu} \omega_{i\delta} + \sum_{ij\alpha\gamma} G_{ij\alpha\gamma} \eta_l(i) m_{i\alpha} m_{j\gamma} + \\
& \sum_{ij} K_{ij} (\boldsymbol{\omega}_i - \boldsymbol{\omega}_j) \cdot (\mathbf{m}_i \times \mathbf{m}_j) - \\
& C \sum_{ij} (\mathbf{u}_i \times \hat{\mathbf{e}}_{ij}) \cdot (\mathbf{m}_i \times \mathbf{m}_j).
\end{aligned} \tag{1}
$$

The first term in the above expression represents magnetic dipolar interaction. The second term is the magnetic exchange coupling between magnetic moments up to third NN. The third, fourth and fifth terms characterize the change in magnetic exchange interaction induced by the local modes, AFD motions, and strains. Note that the first five energies can only lead to collinear magnetism. On the other hand, the sixth term, which involves AFD tiltings and in which the j index runs over the six first NN of site i, is responsible for the spin-canted weak magnetization of BFO[27–30]. The last term characterizes the inverse spin-current model[5,6]. Note that sites i and j were assumed to be second NN in Refs.[7,21] in this last term, which allows to reproduce the $[1\bar{1}0]$ propagation direction (a second NN direction) of the magnetic cycloid of bulk BFO.

However, in terms of strength, it appears to be counter intuitive that the first NN interactions are ignored in the inverse spin-current model. We thus now decide to consider both the first- and second-nearest neighbors, such that the spin current model can be rewritten as

$$
\begin{aligned}
\Delta E = & -C_1 \textstyle\sum_{ij}^{1^{\text{st}}\text{NN}} (\mathbf{u}_i \times \hat{\mathbf{e}}_{ij}) \cdot (\mathbf{m}_i \times \mathbf{m}_j) \\
& - C_2 \textstyle\sum_{ij}^{2^{\text{nd}}\text{NN}} (\mathbf{u}_i \times \hat{\mathbf{e}}_{ij}) \cdot (\mathbf{m}_i \times \mathbf{m}_j) \,,
\end{aligned} \tag{2}
$$

in which the j sites of the first sum are (the six) first NN of site i, and $\hat{\mathbf{e}}_{ij}$ is a unit vector lying along the different $\langle 100\rangle$ pseudo-cubic (PC) directions, and the j sites of the second sum are (the twelve) second NN of site i, which results in $\hat{\mathbf{e}}_{ij}$ being a unit vector lying along the different $\langle 110\rangle$ PC directions, respectively. Note that Ref.[20] only adopted the first NN choice. On the other hand, in our simulations, both C_1 and C_2 are allowed to vary to construct a novel magnetic phase diagram. Other parameters in the effective Hamiltonian are obtained from first-principles density functional calculations.

We carry out Monte Carlo (MC) simulations with 12×12×12 supercells, in terms of the 5-atom perovskite unit cells. For any given selected set of (C_1, C_2) coefficients, all the degrees of freedom are allowed to relax, corresponding to the unstrained bulk. To find the stable magnetic structure, we equilibrate the system starting from different magnetic structures in the $R3c$ phase at 10 K[31] for 80,000 sweeps. Note that the resulting structures remain $R3c$ or with small distortions for large C_1/C_2 due to the slightly broken symmetry by the magnetic structure, as described in Ref.[19]. In the following, we focus on the magnetic configurations. A magnetic phase diagram is determined by finding the spin structure with the lowest energy, as plotted in Fig. 1a. The spin structure and propagation direction of cycloids are determined by computing the discrete Fourier transform (FT) of the magnetic moments for the supercell[32]. For cycloids, box size and periodic boundary conditions impose a cycloidal period that must be accommodated by the supercell; therefore, compared with reality, quantitatively the obtained C values are expected to be larger due to reduced modulation length scale. However, this should not cause qualitative effect on the predicted phase diagram, as C_1 and C_2 terms are scaled in the same manner.

III. RESULTS AND DISCUSSION

Several features can be seen from this phase diagram. First, the G-AFM state is the ground state if $C_1 = C_2 = 0$, because the spin current term in Eq. 1 vanishes, and the other terms favor a homogeneous AFM structure (with weak magnetization). This corresponds to the R point $\boldsymbol{k}_{\text{AFM}} = (2\pi/a)(1/2, 1/2, 1/2)$ from the

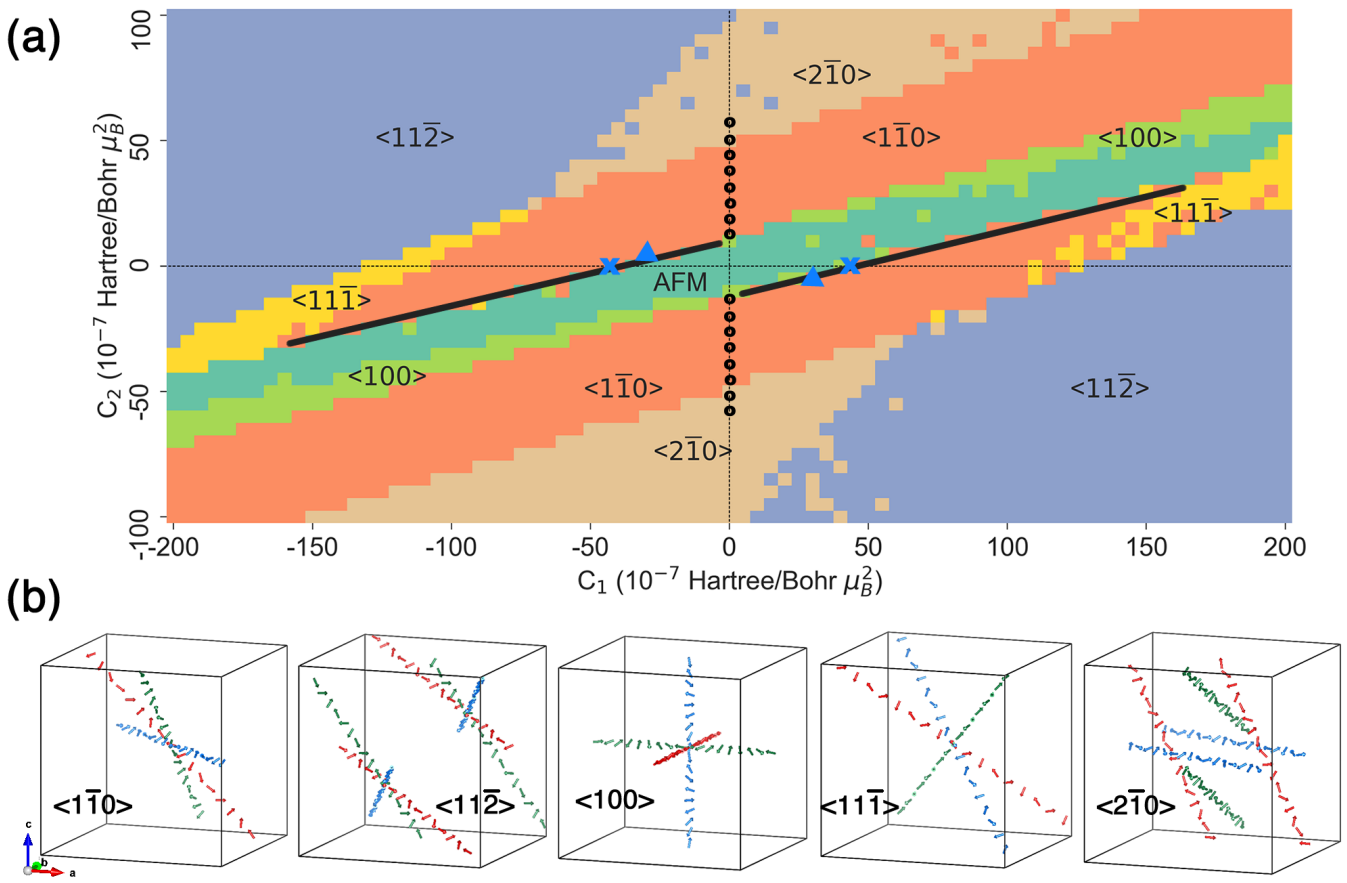

FIG. 1. Predicted magnetic structures at various C_1 and C_2 values for bulk BFO. (a) Calculated phase diagram as functions of C_1 and C_2[33]. For the $< 1\bar{1}0 >$ cycloid, the blue cross symbols are the C_1 value converted from Ref.[20] (with C_2=0); circles are the C_2 values in Ref.[19] (with C_1=0); the blue triangle symbols are calculated by density functional theory[39]. The black lines are determined by considering the critical magnetic field of 18 T changing the $[1\bar{1}0]$ cycloid to AFM. (b) Illustration of the propagation directions of the five types of cycloids. For each type, equivalent cycloids of different propagation directions are shown in red, blue, and yellow colors.

FT, where a is the PC lattice constant. Next, for some finite C values, cycloid magnetic structures can be more stable. In fact, *five* types of cycloids show up in the phase diagram, with different propagation directions as illustrated in Fig. 1b. More precisely, when increasing C_1 with $C_2 = 0$, a sequence of different types of cycloids occur, with their propagation directions being $< 100 >$, $< 1\bar{1}0 >$, $< 11\bar{1} >$, and $< 11\bar{2} >$, which include the experimentally observed type-1 and type-2 cycloids. On the other hand, if increasing C_2 with $C_1 = 0$, the sequence is $< 100 >$, $< 1\bar{1}0 >$, $< 2\bar{1}0 >$, and $< 11\bar{2} >$, again including the type-1 and type-2 cycloids.

Previous reports showed that type-1 cycloid can be explained with only 1st NN terms (C_2=0)[20] or only 2nd NN terms (C_1=0)[7,19] for the spin current model. This is in line with our predictions, and the reported values are consistent with our phase diagram, as shown by discrete symbols (crosses and circles) in Fig. 1a. With solely 1st NN or 2nd NN terms, type-2 cycloid can also be the ground state, except that the required C_1 or C_2 values are much larger than those for type-1 cycloid.

TABLE I. Reciprocal $\boldsymbol{k}$ vectors from Fourier transform of the magnetic structures for a 12×12×12 supercell, in terms of $2\pi/a$, where a is the PC lattice constant.

	G-AFM				
$\boldsymbol{k}$	$(\frac{1}{2}, \frac{1}{2}, \frac{1}{2})$				
	Cycloid propagation direction				
	[100]	[1$\bar{1}$0]	[11$\bar{2}$]	[11$\bar{1}$]	[2$\bar{1}$0]
$\boldsymbol{k}$	$(\frac{7}{12}, \frac{1}{2}, \frac{1}{2})$	$(\frac{7}{12}, \frac{5}{12}, \frac{1}{2})$	$(\frac{7}{12}, \frac{7}{12}, \frac{4}{12})$	$(\frac{7}{12}, \frac{7}{12}, \frac{5}{12})$	$(\frac{8}{12}, \frac{5}{12}, \frac{1}{2})$

Among the other three types of cycloids, the $< 2\bar{1}0 >$ cycloid that was predicted in Ref.[19] is also reproduced here. More interestingly, two new types of cycloids with $< 100 >$ and $< 11\bar{1} >$ propagation directions are found to be stable near the AFM, type-1 and type-2 cycloid states. We are not aware that these two latter magnetic configurations have ever been mentioned in previous literature. In contrast to the type-1 and type-2 cycloids,

the $< 2\bar{1}0 >$, $< 100 >$ and $< 11\bar{1} >$ cycloids have propagation directions no longer perpendicular to the polarization, causing $\mathbf{P}$ to deviate slightly from the [111] direction, as previously described in Ref.[19]. For all five types of cycloids, the magnetic moments rotate mainly in the plane of the polarization and the propagation vector. Small out-of-plane components, known as the spin density wave, also occur in all cases, being consistent with former studies[7,19,20].

The $\boldsymbol{k}$ vector from the FT of these magnetic structures are listed in Table I. Since $\boldsymbol{k}$ of these cycloids are close to the R point in reciprocal space, magnetic structures of the cycloids are close to the G-type AFM ordering, as one would expect for BFO, where the AFM 1st NN exchange interaction is dominant[20]. It is also intuitive to note that, in general, an increasing C_1 (or C_2) causes increasing deviation from G-AFM, indicated by the deviation of $\boldsymbol{k}$ from the R point.

When C_1 and C_2 are both finite, it is worth to point out that C_1 and C_2 terms in Eq. 2 have opposite contributions if these two coefficients have the same signs (top right and bottom left quadrants in Fig. 1a), as the 1st NNs are antiferromagnetically ordered, while the 2nd NNs are ferromagnetically ordered within a G-type AFM structure. Therefore, one can understand that the AFM state remains continuously stable in both the bottom left and top right quadrants of Fig. 1a, within a band inside which the C_1 and C_2 coefficients concomitantly increase. Note also that if, on the other hand, C_1 and C_2 have opposite signs (bottom right and top left quadrants in Fig. 1a), the contributions are collaborative. This difference between (C_1,C_2) having opposite signs in the bottom right and top left quadrants *versus* being of the same sign in the top right and bottom left quadrants also govern the shape of the bands that are associated with each of the five cycloids. For instance, for any of the five cycloidal phases, continuous bands, for which C_1 and C_2 coefficients increase together, exist throughout the whole phase diagram. Note also that an inversion symmetry can be identified in the phase diagram, as reversing the signs of both C_1 and C_2 should yield identical result according to Eq. 2 (when reverting $\mathbf{m}_i \times \mathbf{m}_j$ within the same type of cycloid)[34].

Next we demonstrate how different cycloidal propagation directions can be generated by the 1st and 2nd NN contributions that are along $< 100 >$ and $< 110 >$ directions, respectively. In fact, for each type of cycloid, $\mathbf{m}_i \times \mathbf{m}_j$ for any 1st or 2nd NN pair of i and j are in the same (or opposite) directions, which can be quantified as $w_{ij}\boldsymbol{\xi}$, with w_{ij} being the weight of a common vector $\boldsymbol{\xi}$. Therefore, each term in Eq. 2 can be rewritten as

$$\Delta E = -C_{1,2}\mathbf{u} \cdot (\sum_{ij} w_{ij}\hat{\mathbf{e}}_{ij}) \times \boldsymbol{\xi} \ , \qquad (3)$$

where $C_{1,2}$ represents C_1 or C_2, and the propagation vector $\boldsymbol{q}$ can naturally be seen as the weighted sum of $\hat{\mathbf{e}}_{ij}$, i.e., $\sum_{ij} w_{ij}\hat{\mathbf{e}}_{ij}$. The weights for each pair of neighbors are given in Table II. What is remarkable is that different individual solutions of the 1st NN and 2nd NN spin-current models coexist with different weights (in magnitude and even sign), and "work together", to create these magnetic cycloids. For instance, the type-2 cycloid with the $[11\bar{2}]$ propagation direction is contributed by 1st NN solutions along the [100] (or $[\bar{1}00]$), [010] (or $[0\bar{1}0]$), and [001] (or $[00\bar{1}]$) directions with their weights in the proportion of $1:1:-2$, respectively, exactly resulting in the weighted sum of $[11\bar{2}]$. The contribution from the 2nd NN consists of solutions corresponding to [011] ($[0\bar{1}\bar{1}]$), $[01\bar{1}]$ (or $[0\bar{1}1]$), [101] (or $[\bar{1}0\bar{1}]$), $[10\bar{1}]$ (or $[\bar{1}01]$), [110] (or $[\bar{1}\bar{1}0]$), and $[1\bar{1}0]$ (or $[\bar{1}10]$)] directions with weights in the proportion of $-1:2:-1:2:2:0$, respectively, again resulting in the weighted sum of $[11\bar{2}]$. For the previously overlooked $[11\bar{1}]$ cycloid, the corresponding weights are $1:1:-1$ for the 1st NN, and $0:1:0:1:1:0$ for the 2nd NN, therefore giving rise to the $[11\bar{1}]$ propagation direction. Note that whether C_1 and C_2 have the same or opposite signs, they yield the same propagation direction. Moreover, we note that an increasing contribution from the neighbors can be seen as the cycloid has increasing deviation from the G-AFM state.

TABLE II. Decomposition of contributions to the propagation direction from the 1st and 2nd nearest neighbors in the spin current model. Note that opposite neighboring terms (e.g., 100 and $\bar{1}00$) have the same contribution.

		G-AFM	Propagation direction				
			[100]	$[1\bar{1}0]$	$[11\bar{2}]$	$[11\bar{1}]$	$[2\bar{1}0]$
C_1	100 or $\bar{1}00$	0	1	1	1	1	2
	010 or $0\bar{1}0$	0	0	−1	1	1	−1
	001 or $00\bar{1}$	0	0	0	−2	−1	0
C_2	011 or $0\bar{1}\bar{1}$	0	0	−1	−1	0	−1
	$01\bar{1}$ or $0\bar{1}1$	0	0	−1	2	1	−1
	101 or $\bar{1}0\bar{1}$	0	1	1	−1	0	2
	$10\bar{1}$ or $\bar{1}01$	0	1	1	2	1	2
	110 or $\bar{1}\bar{1}0$	0	1	0	2	1	1
	$1\bar{1}0$ or $\bar{1}10$	0	1	2	0	0	3

Now we discuss what values of C_1 and C_2 BFO may take in reality. The first consideration comes from the experimental evidence that the type-1 cycloid transits into the G-AFM state under a critical magnetic field of 18 T applied along the [11-2] direction in bulk BFO[11,35,36]. We numerically found that this requires type-1 cycloid and AFM state to have a shared boundary, and the resulting possible C values are shown as black lines in Fig. 1a. These allowed values are very close to the boundary, only slightly favoring the type-1 cycloid, since magnetic field only causes a very small change to the energy difference between these two states, which is about two order of magnitude smaller than the energy of the sole spin current term. We have also calculated the DM interaction parameters from density function theory (DFT) using the four-state method[37,38] (more details of the DFT results

will be reported in a separate article[39]). The first and second NN DM interaction parameters for the spin-current term are 0.102 and 0.021 meV, respectively, which can be converted to C_1 and C_2 as 29.9×10^{-7} and -5.04×10^{-7} Hartree/(Bohr$\cdot\mu_B^2$), respectively. The magnitude of the ratio of C_1/C_2 found by these DFT calculations is therefore about 5.9, indicating that contribution from the second NN is not negligible. Interestingly, these DFT values lie very close to the black line of possible C values predicted by the phase diagram (Fig. 1a). They are also very close to a region of stability of cycloids having a $< 100 >$ propagation direction, suggesting that this latter presently unknown cycloid may be observed by varying some factors, such as strains, pressure, alloying, surface termination, etc.

Further insight for the C_1/C_2 values can be obtained from the existence of type-2 cycloid found in experiments in slightly strained thin films[8,17,18]. Within the considered C values based on the critical magnetic field, the best C_1 and C_2 that allow the energy to be close to $< 11\bar{2} >$ or $< 11\bar{1} >$ cycloid is around $C_1 \sim 150\times10^{-7}$ Hartree/(Bohr$\cdot\mu_B^2$) and $C_2 \sim 30\times10^{-7}$ Hartree/(Bohr$\cdot\mu_B^2$), which is close to the triple point, where the AFM phase, type-1 cycloid and $< 11\bar{1} >$ cycloid have the same energies. Such fact strongly suggests that the $< 11\bar{1} >$ cycloid may occur in BFO under certain conditions, for its proximity in energy with the AFM, type-1, and type-2 cycloids, as the later three states are energetically close and are observed with rather small strain changes.

Nevertheless, we would like to point out that, in practice, the type-2 cycloid observed in BFO films may involve effects beyond epitaxial strain. As a matter of fact, the energy difference between any two phases caused by strain is relatively small compared with the spin current energy. As the $< 11\bar{2} >$ cycloid is separated from the AFM state (by $< 11\bar{1} >$ and $< 1\bar{1}0 >$ cycloids), only considering strain effect could not explain its existence, unless type-2 cycloid is in fact the $< 11\bar{1} >$ cycloid. Surface effect may, e.g., play an important role here, which may be responsible for the experimental stabilization of the $< 11\bar{2} >$ cycloid.

IV. CONCLUSIONS

In summary, we have predicted a magnetic phase diagram for bulk BFO, as functions of first- and second-nearest-neighbor interaction strength in the spin current model, by using a state-of-the-art first-principles-based effective Hamiltonian method. In contrast with previous models, we found that both first- and second-nearest-neighbor interactions have to be taken into account, in order to reproduce the different spin structures that have been observed so far. Previously unknown types of cycloids are found in this phase diagram, including one having a propagation direction along $[1\bar{1}\bar{1}]$ and that may explain recent experiments. Further, we provided an unprecedented microscopic insight into the formation of the different cycloids that can form in BFO, by revealing and analyzing how the single solutions of the spin current model "work" together to create such complex magnetic arrangements and how the first and second nearest-neighbor terms compete or collaborate (depending on their signs) to yield the phase diagram.

Finally, we emphasize that although DM interaction can be studied by DFT with a certain precision, it is always interesting to explore the region in the vicinity of the calculated value to understand (i) the stability of the magnetic state that is found, and (ii) the different phases if the DM interaction is, e.g., tuned by strain, chemical doping, surface termination, etc. In particular, the predicted magnetic phase diagram can in fact not only be applied to BFO, but be readily generalized to other multiferroics that are ferroelectric and antiferromagnetic. Similar to BFO, both first- and second-nearest-neighbor interactions would need to be considered, and more interestingly, triple and quadruple points where three or four magnetic configurations that are energetically degenerate may be realized. It opens new perspectives to find systems in the vicinity of these points, such that the competing phases may induce novel magnetic structures. We hope that our work will motivate further experiments to unveil new types of magnetic cycloids and novel topological structures in multiferroics.

ACKNOWLEDGMENTS

We thank M. Viret and C. Paillard for insightful discussions. B.X. thanks the support of the Air Force Office of Scientific Research under Grant No. FA9550-16-1-0065. L.B. acknowledges the DARPA Grant No. HR0011727183?D18AP00010 (TEE program). We also thank the computational support from Arkansas High Performance Computer Center at the University of Arkansas.

* Email address: xubin.physics@gmail.com
† Email address: laurent@uark.edu

[1] I. Dzyaloshinsky, J. Phys. Chem. Solids **4**, 241 (1958).
[2] T. Moriya, Phys. Rev. Lett. **4**, 228 (1960).
[3] A. Glazer, Acta Crystallographica Section B: Structural Crystallography and Crystal Chemistry **28**, 3384 (1972).
[4] I. Sosnowska, T. P. Neumaier, and E. Steichele, J. Phys. C: Solid State Phys. **15**, 4835 (1982).
[5] H. Katsura, N. Nagaosa, and A. V. Balatsky, Phys. Rev. Lett. **95**, 057205 (2005).
[6] A. Raeliarijaona, S. Singh, H. Fu, and L. Bellaiche, Phys. Rev. Lett. **110**, 137205 (2013).

[7] D. Rahmedov, D. Wang, J. Íñiguez, and L. Bellaiche, Phys. Rev. Lett. **109**, 037207 (2012).
[8] D. Sando, A. Agbelele, D. Rahmedov, J. Liu, P. Rovillain, C. Toulouse, I. Infante, A. Pyatakov, S. Fusil, E. Jacquet, *et al.*, Nat. Mater. **12**, 641 (2013).
[9] Y. F. Popov, A. Zvezdin, G. Vorob'ev, A. Kadomtseva, V. Murashev, and D. Rakov, JETP Lett. **57**, 65 (1993).
[10] Y. F. Popov, A. Kadomtseva, G. Vorob'Ev, and A. Zvezdin, Ferroelectrics **162**, 135 (1994).
[11] M. Tokunaga, M. Azuma, and Y. Shimakawa, J. Phys. Soc. Jpn. **79**, 064713 (2010).
[12] A. Agbelele, D. Sando, C. Toulouse, C. Paillard, R. Johnson, R. Rüffer, A. Popkov, C. Carrétéro, P. Rovillain, J.-M. Le Breton, *et al.*, Adv. Mater. **29** (2017).
[13] P. Rovillain, R. De Sousa, Y. t. Gallais, A. Sacuto, M. Méasson, D. Colson, A. Forget, M. Bibes, A. Barthélémy, and M. Cazayous, Nat. Mater. **9**, 975 (2010).
[14] A. Popkov, N. Kulagin, S. Soloviov, K. Sukmanova, Z. Gareeva, and A. Zvezdin, Phys. Rev. B **92**, 140414 (2015).
[15] I. Sosnowska, W. Schäfer, W. Kockelmann, K. Andersen, and I. Troyanchuk, Appl. Phys. A **74**, s1040 (2002).
[16] J. Buhot, C. Toulouse, Y. Gallais, A. Sacuto, R. De Sousa, D. Wang, L. Bellaiche, M. Bibes, A. Barthélémy, A. Forget, *et al.*, Phys. Rev. Lett. **115**, 267204 (2015).
[17] W. Ratcliff, D. Kan, W. Chen, S. Watson, S. Chi, R. Erwin, G. J. McIntyre, S. C. Capelli, and I. Takeuchi, Adv. Funct. Mater. **21**, 1567 (2011).
[18] S. Burns, D. Sando, B. Xu, B. Dupé, L. Russell, G. Deng, J. Seidel, L. Bellaiche, V. Nagarajan, and C. Ulrich, (unpublished).
[19] S. Bhattacharjee, D. Rahmedov, L. Bellaiche, and D. Wang, MRS Communications **3**, 213 (2013).
[20] R. S. Fishman, arXiv:1708.04925 (2017).
[21] R. S. Fishman, J. T. Haraldsen, N. Furukawa, and S. Miyahara, Phys. Rev. B **87**, 134416 (2013).
[22] W. Zhong, D. Vanderbilt, and K. M. Rabe, Phys. Rev. Lett. **73**, 1861 (1994).
[23] W. Zhong, D. Vanderbilt, and K. M. Rabe, Phys. Rev. B **52**, 6301 (1995).
[24] I. A. Kornev, L. Bellaiche, P.-E. Janolin, B. Dkhil, and E. Suard, Phys. Rev. Lett. **97**, 157601 (2006).
[25] J. B. Neaton, C. Ederer, U. V. Waghmare, N. A. Spaldin, and K. M. Rabe, Phys. Rev. B **71**, 014113 (2005).
[26] P. Fischer, M. Polomska, I. Sosnowska, and M. Szymanski, J. Phys. C: Solid State Phys. **13**, 1931 (1980).
[27] D. Albrecht, S. Lisenkov, W. Ren, D. Rahmedov, I. A. Kornev, and L. Bellaiche, Phys. Rev. B **81**, 140401 (2010).
[28] C. Ederer and N. A. Spaldin, Phys. Rev. B **71**, 060401 (2005).
[29] L. Bellaiche, Z. Gui, and I. A. Kornev, J. Phys. Condens. Matter **24**, 312201 (2012).
[30] D. Wang, J. Weerasinghe, and L. Bellaiche, Phys. Rev. Lett. **109**, 067203 (2012).
[31] Note that this low temperature is chosen for better statistics.
[32] A. M. George, J. Íñiguez, and L. Bellaiche, Phys. Rev. B **65**, 180301(R) (2002).
[33] Some scattered data are due to close energy of the competing phases.
[34] The slight asymmetry is due to numerical errors.
[35] D. Wardecki, R. Przenioslo, I. Sosnowska, Y. Skourski, and M. Loewenhaupt, J. Phys. Soc. Jpn. **77**, 103709 (2008).
[36] M. Viret, Private communication.
[37] H. Xiang, C. Lee, H.-J. Koo, X. Gong, and M.-H. Whangbo, Dalton Trans. 42, 823 (2013).
[38] H. Xiang, E. Kan, S.-H. Wei, M.-H. Whangbo, and X. Gong, Phys. Rev. B 84, 224429 (2011).
[39] C. Xu, B. Xu, B. Dupé, H. Xiang, and L. Bellaiche. (unpublished).